Structural identification of graphene films and nanoislands on 6H-SiC(0001) by direct height measurement

Hamza Ichou, Mohanad Alchaar, Bulent Baris, Adrien Michon, Roy Dagher, Erik Dujardin, David Martrou

Structural identification of graphene films and nanoislands on 6H-SiC(0001) by direct height measurement

Hamza Ichou [1], Mohanad Alchaar [1], Bulent Baris [1], Adrien Michon [2], Roy Dagher [2], Erik Dujardin [1], David Martrou [1]

[1] CEMES, 29 rue Jeanne Marvig, 31400 Toulouse, France

[2] Université Côte d'Azur, CNRS, CRHEA, Valbonne 06560, France

E-mail: Hamza.ichou@cemes.fr (Corresponding Author)

E-mail: David.martrou@cemes.fr (Corresponding Author)

Abstract. 111111111By combining non-contact atomic force microscopy (nc-AFM) and Kelvin probe microscopy (KPFM) in ultra high vacuum environment (UHV), we directly measure the height and work function of graphene monolayer on the Si-face of 6H-SiC(0001) with a precision that allows us to differentiate three different types of graphene structures : Zero layer graphene (ZLG), Quasi free-standing monolayer graphene (QFMLG) and bilayer graphene (BLG). The height and work function of ZLG are 2.62 ± 0.22 Å and 4.42 ± 0.05 eV respectively, when they are 4.09 ± 0.11 Å and 4.63 ± 0.05 eV for QFMLG. The work function is 4.83 ± 0.05 eV for the BLG. Unlike any other available technique, the local nc-AFM/KPFM dual probe makes it possible to directly identify the nature of nanometer-sized graphene islands that constitute the early nuclei of graphene monolayer grown on 6H-SiC(0001) by chemical vapor deposition.

Keywords: Graphene, 6H-SiC, island, ZLG, QFMLG, Submitted to: *Nanotechnology*

1. Introduction:

Graphene draws most of its intrinsic structural and electronic properties from the two-dimensional crystalline ordering of sp^2-bonded carbon atoms on a honeycomb lattice [1, 2, 3, 4]. While the in-plane organization of the σ bonds between carbon atoms is robust, graphene easily adopts different morphologies and electronic properties by engaging transverse interactions with its near-field environment through the available π electrons [5, 6]. One extreme case where subtle structural variations of graphene coexist and have a major effect on their respective electronic behavior is epitaxial graphene on SiC. The first carbon-rich layer formed on the Si-face of SiC(0001) is known as the buffer layer or zero layer graphene (ZLG) [7] that consists of a honeycomb lattice of carbon atoms. In this structure, about 30% of carbon atoms are covalently bound to Si atoms of the SiC substrate [8, 9]. When another carbon layer is formed on top of the ZLG, it is free of any covalent interlayer bonds and electronically behaves as monolayer graphene. It is known as the epitaxial monolayer graphene (EMLG). While the ZLG effectively decouples the EMLG from the SiC substrate, it induces a significant intrinsic doping, which strongly reduces the charge mobility in the EMLG [10, 11]. In order to reduce the ZLG effect on the EMLG, the SiC substrate can be passivated with hydrogen. The resulting graphene layer, named "quasi free standing monolayer" (QFMLG), is decoupled from the substrate and remains undoped [12].

The identification of the graphene structures on the SiC(0001) substrate even at an early stage of growth is tremendously important as it determines its final structural and electronic properties. Numerous experimental techniques and numerical methods have been applied and sometimes combined to elucidate the detailed structure of graphene, such as scanning tunneling microscopy (STM) [13, 14], Kelvin probe force microscopy (KPFM) [15], transmission electron microscopy (TEM) [14], high-resolution X-ray reflectivity (XRR) [16], normal incidence x-ray standing wave (NIXSW) [17], x-ray standing wave excited photo-electron spectroscopy (XSW-XPS) [16, 18], density functional theory (DFT) [17] and ab initio [9] calculations. Figure 1 presents the possible graphene configurations that can be found on the surface of the 6H-SiC(0001) and the associated heights as predicted by DFT calculation based on NIXSW data [17] None of these configurations is energetically favored which usually results in a coexistence of several of them. The identification of the actual structure of a specific graphene zone thus remains a challenge as most direct methods are providing a spatial average of the structural parameters but fail to determine the graphene type of nanometric graphene nuclei.

In this work, we present the characterization of the 6H-SiC(0001) surface after the growth of a graphene layer or of the nucleation graphene nano-islands using UHV non-contact atomic force microscopy coupled to Kelvin probe force microscopy [19, 20]. We demonstrate the presence of zero layer graphene and epitaxial monolayer graphene zones. The standard characterization methods discussed above remain insufficient to determine the graphene island types due to their nanoscale dimensions. Based on direct

height and work function measurements, we are now able to identify the nature of sub-100 nm graphene nucleation islands present on the 6H-SiC(0001) surface after a well-controlled CVD growth process. This structural characterization of graphene nuclei is of paramount interest for optimized graphene growth for future applications [21, 22].

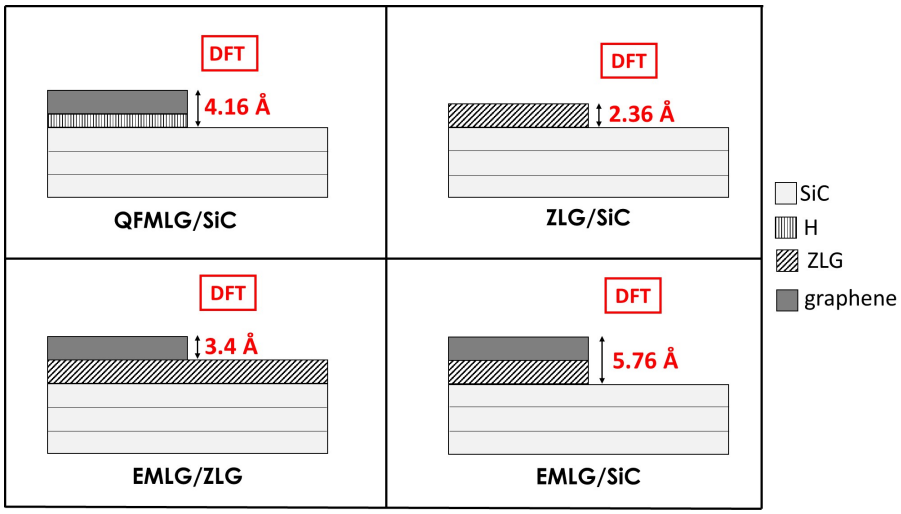

Figure 1: Possible configurations obtained using DFT calculations and NIXSW measurements from the work in reference [17].

2. Experimental details

In this work, two samples produced by two techniques were used and compared . The first one, Sublim-GL, graphene layers on large terraces of 6H-SiC(0001) ($\rho = 1.2 \times 10^{11}$ Ω.cm, thickness = 500.4 μm, size = 8x8 mm^2) were obtained by high temperature sublimation processes. The Raman spectroscopy analysis shows the well-resolved graphite 2D and G bands around 2750 cm^{-1}, which suggest a predominance of sp^2 carbon atoms [SM]. The second one, CVD-GNI, were prepared using propane/hydrogen CVD [23, 24]. The presence of hydrogen in the gas phase promotes Si excess on the surface, hence making impossible graphene growth without propane flow [25]. The growth was done under H_2 and Ar laminar flows of 2 and 10 slm, respectively, under a pressure regulated at 800 mbar. After the ramp-up to the growth temperature of 1450°C and a 3 minutes annealing, graphene was grown by adding 5 sccm of propane in the gas phase for only 2 minutes. This interrupted growth procedure leads to the formation of small nano-islands directly on SiC substrate. After growth, the samples were cooled down to room temperature under H_2 and Ar in 20 minutes.

Height measurements were carried out by non-contact atomic force microscopy (nc-AFM) [26] and the work functions were measured simultaneously by Kelvin probe microscopy (KPFM) [27] at room temperature in ultra-high vacuum. Platinum-Iridium (PtIr) nc-AFM cantilevers, purchased from Nanosensors [28], have a resonance frequency of $f_0 = 300$ kHz, a nominal stiffness of $k = 42$ N/m, and a quality factor

of around 30000. For calibration measurements, we use a HOPG (Highly Oriented Pyrolithic Graphite) substrate sample.

To perform measurements in the frequency modulated KPFM mode [20], a modulation of the amplitude of $U_{KPFM}^{mod} = 500\ mV$ and frequency of 957 Hz is added to the bias voltage U_{bias}. The Kelvin feedback loop brings V to the Kelvin voltage U*(X,Y) that minimizes Δf at each point (X, Y) on the surface. Two images of the surface are recorded simultaneously, the topography image Z(X, Y) and the Kelvin image U*(X,Y).

On a metal surface, U*(X,Y) can be related to the difference between the work function of the tip ϕ_{tip} and the work function of the sample ϕ_{sample}. Note that KPFM is performed with the tip grounded while the bias voltage is applied to the sample, hence U*(X,Y)= $(\phi_{tip} - \phi_{HOPG})/q$, where $q > 0$ is the elementary charge. The Kelvin voltage of HOPG measured with PtIr tips is U_{HOPG}^{*} = -50 ± 100 mV. Since the work function of HOPG has been measured $\phi_{HOPG} = 4.475 \pm 0.05\ eV$ [29], the tip work function ϕ_{tip} is estimated to 4.4 eV.

3. Results and Discussion

3.1. Height measurements by interpolation :

To extract the height h_i of the different graphene type from the topographic images, we have used a non-linear fitting function $topo(x)$ defined by equation 1 for many profiles of the same topographic image. Fig.2.a shows the graphical representation of the fitting function $topo(x)$ and Fig.2.b an example of this method applied to a topographic profile (black curve) of a step. The height histogram of the accumulated data shows a normal distribution that is fitted with a Gaussian with a standard deviation of less than 0.23Å.

$$topo(x) = b(x) + |h_i| \times \sum_{i=1}^{n} sign(h_i) \times [\frac{1}{2} + \frac{1}{\pi} \times arctan\frac{(x - x_i)}{r}] \qquad (1)$$

where : h_i is the steps height ($h_i > 0$ for up-going steps, $h_i < 0$ for down-going steps), $b(x)$ is the topographic background, x_i is the x-coordinate of the step and r is the widening.

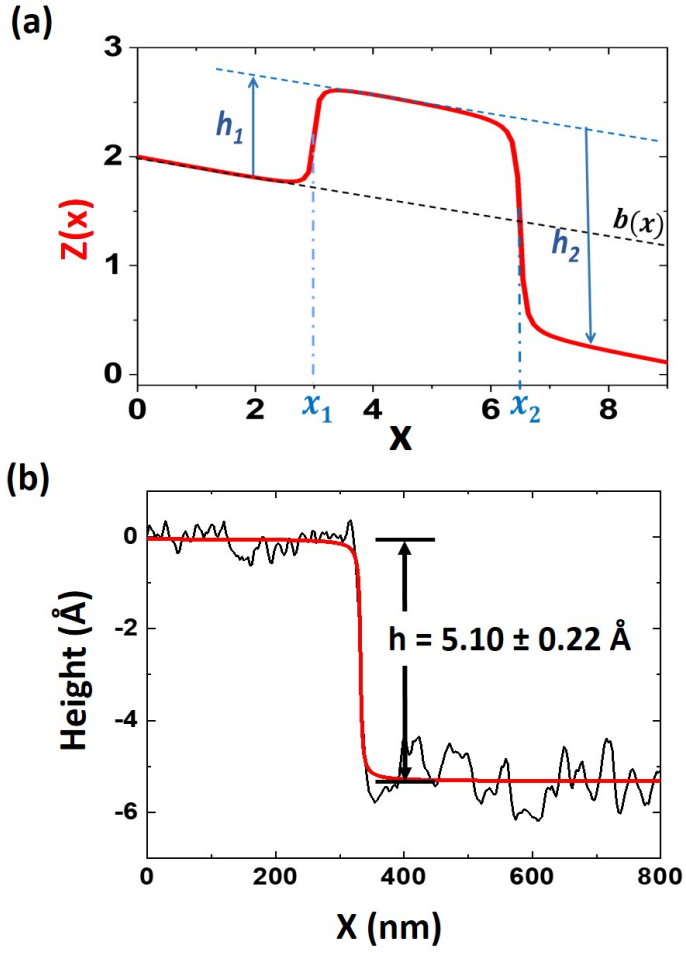

Figure 2: (a) The function $topo(x)$ used for non-linear fitting. (b) Fit (red) realized on a topographic line profile (black).

3.2. Zero layer graphene on SiC: ZLG/SiC

In order to characterize the graphene layer, nc-AFM and KPFM techniques were used. The nc-AFM image in Fig.3.*a* show two distinct regions : dark (low) and bright (high). The black curve in Fig.3.*b* represents one topographic profile (black) and its fit with the function $topo(x)$(red). By analyzing multiple line profiles, we find a histogram which represent the distribution of the heights (Fig.3.*c*), and by a Gaussian fit we find a height step of 5.15 ± 0.22 Å. This distance correlates to the one obtained by DFT calculations (4.88 Å) that corresponds to the height of ZLG together with one Si-C step (2.53 Å), as represented in the schematic model in Fig.3.d [17]. From this result, we can infer the thickness of the ZLG : 2.62 ± 0.22 Å, in good agreement with x-ray standing wave excited photoelectron spectroscopy (XSW-XPS) in conjugation with the STM [13] (2.6 ± 0.4 Å) and x ray reflectivity (XRR) [16] (2.4 ± 0.5 Å).

The surface potential image obtained simultaneously by KPFM clearly shows two different surfaces (Fig.3.e), with a contact potential difference (CPD) of - 372 ± 10 mV

(Fig.3.f). Knowing the CPD of the metallic nc-AFM/KPFM tip (4.4 eV) determined from independent measurements on highly oriented pyrolytic graphite (HOPG) that has a well-defined work function ($4.475 \pm 0.05\ eV$), the work function of the ZLG can be accurately obtained as $4.42 \pm 0.05\ eV$.

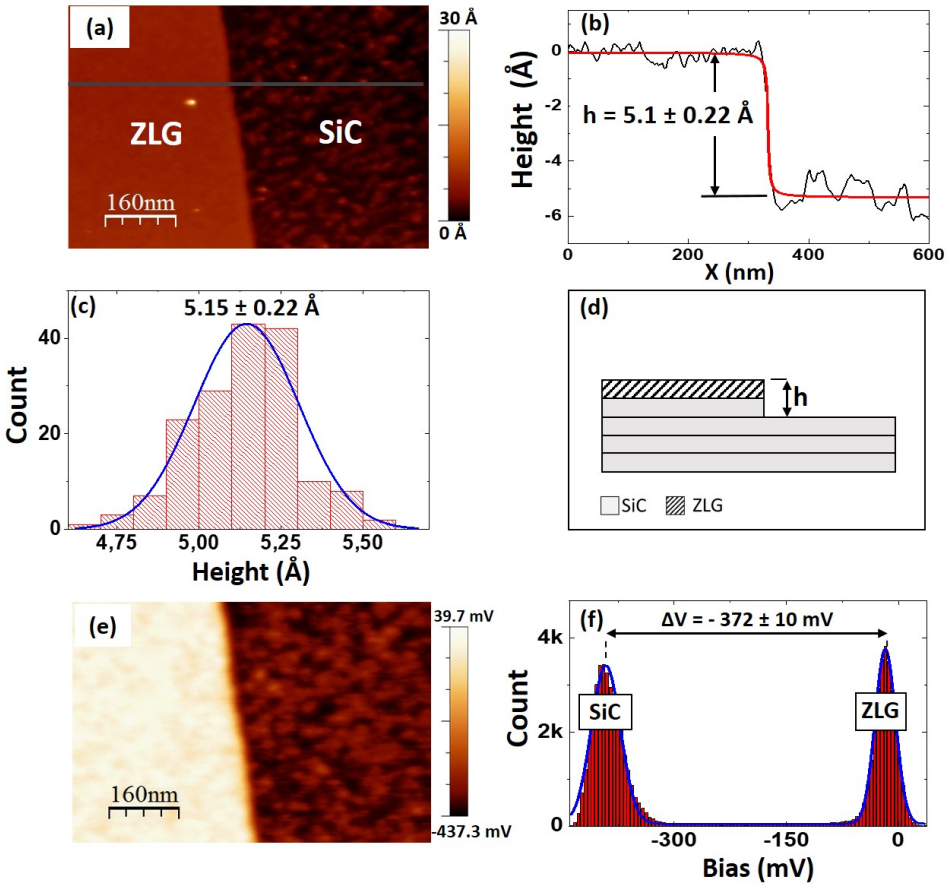

Figure 3: (a) The nc-AFM topography image of the Sublim-GL surface. (b) One line profile (black) of the topographic image and the fitting by the function $topo(x)$ in red. (c) Gaussian fit of the histogram of the line by line profile analysis. (d) Schematic model of the structure. (e) Kelvin potential image. (f) Histogram of the Kelvin potential with corresponding gaussian fits. Image parameters : Size (800×800) nm^2, Amplitude = 5 nm, Δf = -20 Hz, f_{KPFM} = 957 Hz, U^{mod}_{KPFM} = 500 mV.

3.3. Quasi free monolayer graphene (QFMLG) :

In a similar way, we observe in the nc-AFM image in Fig.4.*a*, a step between two regions. The black curve in Fig.4.*b* correspond to the topographic profile and its fitting with the function $topo(x)$ in red. The line by line profile analysis yields the height histogram shown in Fig.4.*c*. We obtain a value of 4.09 ± 0.11 Å that is identified with the QFMLG as shown in the schematic model (Fig.4.*d*), in close agreement with the

DFT calculated values (4.22 ± 0.06 Å) [17]. We note that the height between hydrogen atoms and SiC is not detected with an nc-AFM tip. The contrast in KPFM (Fig.4.e) demonstrates that the surface in the two region is electronically different, with a CPD difference of about 205 ± 10 mV (Fig.4.f). Using the work function of the metallic tip, we find that the work function of the left region is equal to 4.63 ± 0.05 eV which is in close agreement with the results obtained for QFMLG by angle- and time-resolved two-photoelectron spectroscopy [30] (4.65 eV) and Kelvin probe spectroscopy [31] (4.76 ± 0.05 eV).

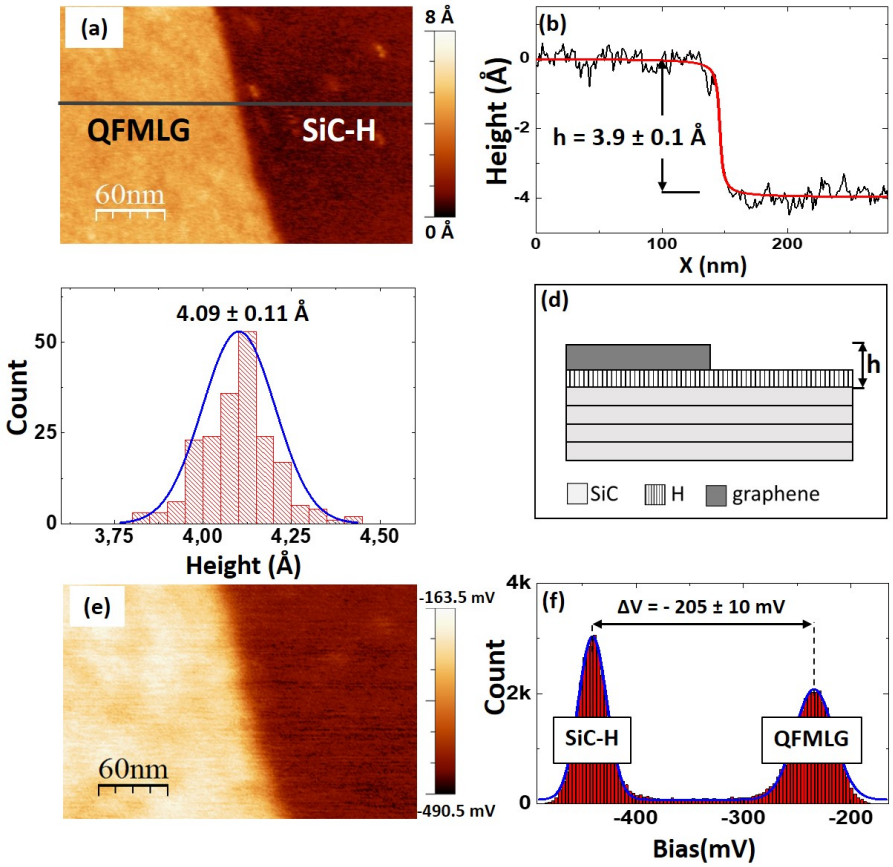

Figure 4: (a) The nc-AFM topography image of the Sublim-GL surface. (b) One line profile (black) of the topographic image and the fitting by the function $topo(x)$(red). (c) Gaussian fit of the histogram of the line by line profile analysis. (d) Schematic model of the structure. (e) Kelvin potential image (f) Histogram of the Kelvin potential with gaussian fits. Image parameters : Size (300 × 300) nm^2, Amplitude = 5 nm, Δf = -20 Hz, f_{KPFM} = 957 Hz, U^{Mod}_{KPFM} = 500 mV.

Table 1: Comparison between the values in the literature and those measured in nc-AFM/KPFM of the height of the different types of graphene and their work function.

	Experiments		References			
Type	Height (Å)	Work function (eV)	Height (Å)		Work function (eV)	
ZLG	2.62 ± 0.22	4.42 ± 0.05	2.6 ± 0.4 2.4 ± 0.5 2.36	[13] [16] [17]	–	
QFMLG	4.09 ± 0.11	4.63 ± 0.05	4.16 4.22 ± 0.06	[17] [17]	4.65 4.79 ± 0.05	[30] [31]

3.4. Graphene nano-islands :

Figure 5 show a large scale AFM image of the synthesized graphene nanoislands grown on SiC substrates with a density of about one nanoisland per square micrometer. All nanosilands appear isolated with typically sub-100nm dimensions.

Standard spectroscopy methods generally used to identify graphene types cannot apply to such nanometric graphene seeds and nanoislands that are formed in the early stages of graphene growth.

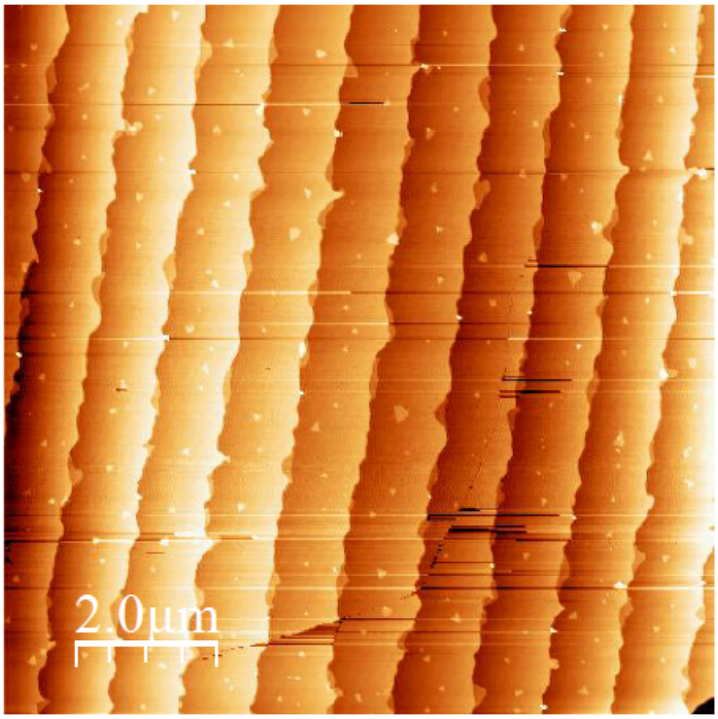

Figure 5: Ambient AFM image of as-synthesized graphene nanoislands grown with a density of about $1\mu m^{-2}$ by CVD on SiC substrates (CVD-GNI).

The nc-AFM/KPFM method demonstrated here constitutes a powerful tool to identify the structural nature of nano-island graphene seeds from the height and work function information. Figures 6.a and 6.b show a small graphene nanoisland on SiC, with the corresponding KPFM image. A triangular graphene nanoisland with a lateral dimension of 60 nm isolated on the upper terrace (Fig.6.c) is analyzed with our method. This upper terrace is identified as ZLG by comparison of the surface roughness and CPD difference with respect to the lower terrace with Figure 3. The black curve in Fig.6.d correspond to the topographic profile and its fit with the function $topo(x)$ in red. The line by line profile yields the height histogram in Fig.6.e. We obtain a value of 3.69 $\pm$ 0.11 Å that corresponds to the height of graphene monolayer on top of the ZLG terrace as shown in the schematic model of Fig.6.f. In Fig.6.g and Fig 6.h the KPFM image shows a negative contrast of the nanoisland with respect to the ZLG layer but also a significant noise level due to the presence of contamination on the edges. Therefore, no quantitative information can be deduced from the Kelvin potential profiles.

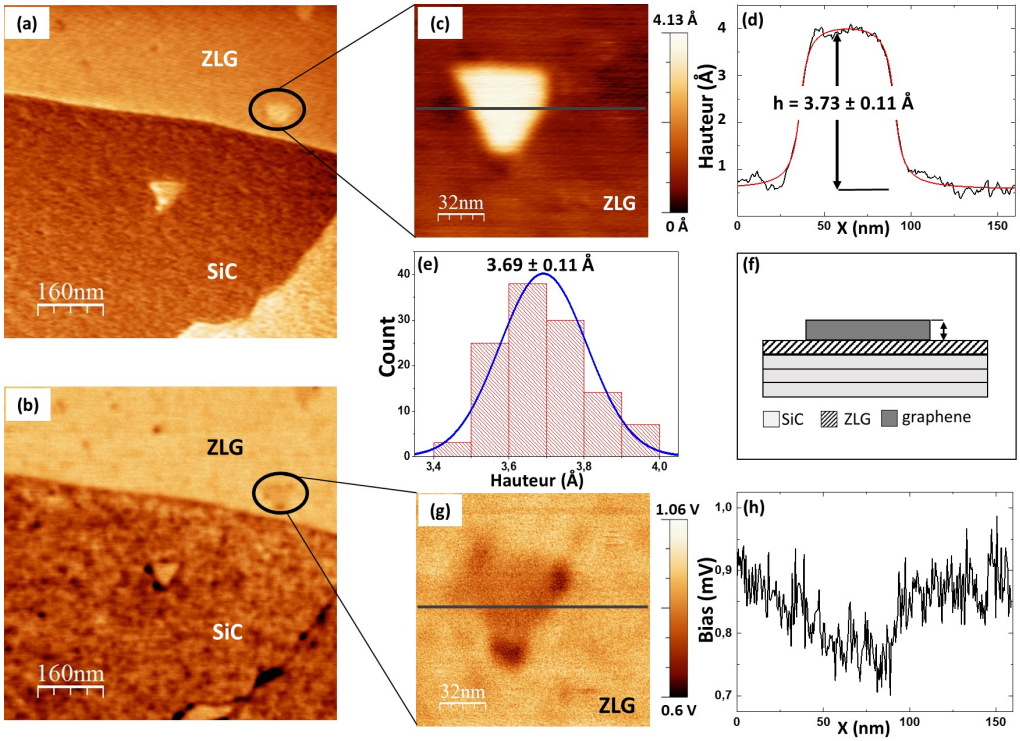

Figure 6: (a) The nc-AFM topography image of a graphene island (CVD-GNI). (b) Experimental data curve of one line profile of the topographic image (black), and the non-linear curve fit (red) given by equation 1. (c) Histogram of the line by line profile analysis with the function $topo(x)$. (d) Schematic model of the structure. (e) Kelvin potential image of graphene island. (f) Kelvin potential profile. Image parameters : Size : (800 $\times$ 800) nm^2 for (a) and 160 $\times$ 160 nm^2 for (c), Amplitude = 5 nm, Δf = -20 Hz, f_{KPFM} = 957 Hz, U^{Mod}_{KPFM} = 1V.

4. Conclusion:

In summary, we have demonstrated that combined nc-AFM and KPFM measurements in UHV enable the direct identification of two graphene structures, ZLG and QFMLG, thanks to a sub-nanometer height accuracy and simultaneous work function determination. We have applied this method to isolated graphene nano-islands, with sub-100 nm lateral size that no standard spectroscopy method would be able to identify. We could assign a structural type in agreement with DFT calculations. Our results provide a reliable and direct method to monitor nanographene on insulating surfaces and reach detailed structural and electronic characterization.

References

[1] Zhang Y, Jiang Z, Small J P, Purewal M S, Tan Y W, Fazlollahi M, Chudow J D, Jaszczak J A, Stormer H L and Kim P 2006 Phys. Rev. Lett. **96**(13) 136806 URL https://link.aps.org/doi/10.1103/PhysRevLett.96.136806

[2] Katsnelson M I, Novoselov K S and Geim A K 2006 Nature Physics **2**(9) 620–625 URL https://doi.org/10.1038/nphys384

[3] Morozov S V, Novoselov K S, Katsnelson M I, Schedin F, Elias D C, Jaszczak J A and Geim A K 2008 Phys. Rev. Lett. **100**(1) 016602 URL https://link.aps.org/doi/10.1103/PhysRevLett.100.016602

[4] Soldano C, Mahmood A and Dujardin E 2010 Carbon **48** 2127–2150 ISSN 0008-6223 URL https://www.sciencedirect.com/science/article/pii/S0008622310000928

[5] Van Bommel A, Crombeen J and Van Tooren A 1975 Surface Science **48** 463–472 ISSN 0039-6028 URL https://www.sciencedirect.com/science/article/pii/0039602875904197

[6] Jernigan G G, VanMil B L, Tedesco J L, Tischler J G, Glaser E R, Anthony Davidson and P M C and Gaskill K D 2009 Nano Lett. **9**(7) 2605–2609

[7] Varchon F, Feng R, Hass J, Li X, Nguyen B N, Naud C, Mallet P, Veuillen J Y, Berger C, Conrad E H and Magaud L 2007 Phys. Rev. Lett. **99**(12) 126805 URL https://link.aps.org/doi/10.1103/PhysRevLett.99.126805

[8] Emtsev K V, Speck F, Seyller T, Ley L and Riley J D 2008 Phys. Rev. B **77**(15) 155303 URL https://link.aps.org/doi/10.1103/PhysRevB.77.155303

[9] Mattausch A and Pankratov O 2007 Phys. Rev. Lett. **99**(7) 076802 URL https://link.aps.org/doi/10.1103/PhysRevLett.99.076802

[10] Ristein J, Mammadov S and Seyller T 2012 Phys. Rev. Lett. **108**(24) 246104 URL https://link.aps.org/doi/10.1103/PhysRevLett.108.246104

[11] Rutter G M, Crain J N, Guisinger N P, Li T, First P N and Stroscio J A 2007 Science **317** 219–222 (*Preprint* https://www.science.org/doi/pdf/10.1126/science.1142882) URL https://www.science.org/doi/abs/10.1126/science.1142882

[12] Riedl C, Coletti C, Iwasaki T, Zakharov A A and Starke U 2009 Phys. Rev. Lett. **103**(24) 246804 URL https://link.aps.org/doi/10.1103/PhysRevLett.103.246804

[13] Rutter G M, Guisinger N P, Crain J N, Jarvis E A A, Stiles M D, Li T, First P N and Stroscio J A 2007 Phys. Rev. B **76**(23) 235416 URL https://link.aps.org/doi/10.1103/PhysRevB.76.235416

[14] Borysiuk J, Bożek R, Strupiński W, Wysmołek A, Grodecki K, Stępniewski R and Baranowski J M 2009 Journal of Applied Physics **105** 023503 (*Preprint* https://doi.org/10.1063/1.3065481) URL https://doi.org/10.1063/1.3065481

[15] Filleter T, Emtsev K V, Seyller T and Bennewitz R 2008 Applied Physics Letters **93**

133117 (*Preprint* https://doi.org/10.1063/1.2993341) URL https://doi.org/10.1063/1.2993341

[16] Emery J D, Detlefs B, Karmel H J, Nyakiti L O, Gaskill D K, Hersam M C, Zegenhagen J and Bedzyk M J 2013 Phys. Rev. Lett. **111**(21) 215501 URL https://link.aps.org/doi/10.1103/PhysRevLett.111.215501

[17] Sforzini J, Nemec L, Denig T, Stadtmüller B, Lee T L, Kumpf C, Soubatch S, Starke U, Rinke P, Blum V, Bocquet F C and Tautz F S 2015 Phys. Rev. Lett. **114**(10) 106804 URL https://link.aps.org/doi/10.1103/PhysRevLett.114.106804

[18] Conrad M, Rault J, Utsumi Y, Garreau Y, Vlad A, Coati A, Rueff J P, Miceli P F and Conrad E H 2017 Phys. Rev. B **96**(19) 195304 URL https://link.aps.org/doi/10.1103/PhysRevB.96.195304

[19] Kitamura S and Iwatsuki M 1998 Applied Physics Letters **72** 3154–3156 (*Preprint* https://doi.org/10.1063/1.121577) URL https://doi.org/10.1063/1.121577

[20] Nonnenmacher M, O'Boyle M P and Wickramasinghe H K 1991 Applied Physics Letters **58** 2921–2923 (*Preprint* https://doi.org/10.1063/1.105227) URL https://doi.org/10.1063/1.105227

[21] Moon J S, Curtis D, Hu M, Wong D, McGuire C, Campbell P M, Jernigan G, Tedesco J L, VanMil B, Myers-Ward R, Eddy C and Gaskill D K 2009 IEEE Electron Device Letters **30** 650–652

[22] Tzalenchuk A, Lara-Avila S, Kalaboukhov A, Paolillo S Syväjärvi M, Yakimova R, Kazakova O, Janssen T, Fal'ko V and Kubatkin S 2010 Nat Nanotechnol. **5** 186–189 URL https://doi.org/10.1038/nnano.2009.474

[23] Michon A, Vézian S, Roudon E, Lefebvre D, Zielinski M, Chassagne T and Portail M 2013 Journal of Applied Physics **113** 203501 (*Preprint* https://doi.org/10.1063/1.4806998) URL https://doi.org/10.1063/1.4806998

[24] Michon A, Vézian S, Ouerghi A, Zielinski M, Chassagne T and Portail M 2010 Applied Physics Letters **97** 171909 (*Preprint* https://doi.org/10.1063/1.3503972) URL https://doi.org/10.1063/1.3503972

[25] Dagher R, Blanquet E, Chatillon C, Journot T, Portail M, Nguyen L, Cordier Y and Michon A 2018 CrystEngComm **20**(26) 3702–3710 URL http://dx.doi.org/10.1039/C8CE00383A

[26] Scienta omicron, taunusstein, germany. URL https://scientaomicron.com/en

[27] Zerweck U, Loppacher C, Otto T, Grafström S and Eng L 2005 Physical Review B **71** 1–9 ISSN 1098-0121 URL http://link.aps.org/doi/10.1103/PhysRevB.71.125424

[28] See the folowing website for more informations about the cantilevers. URL www.nanosensors.com

[29] Hansen W N and Hansen G J 2001 Surface Science **481** 172–184 ISSN 0039-6028 URL https://www.sciencedirect.com/science/article/pii/S0039602801010366

[30] Gugel D, Niesner D, Eickhoff C, Wagner S, Weinelt M and Fauster T 2015 2D Materials **2** 045001 URL https://doi.org/10.1088/2053-1583/2/4/045001

[31] Mammadov S, Ristein J, Krone J, Raidel C, Wanke M, Wiesmann V, Speck F and Seyller T 2017 2D Materials **4** 015043 URL https://doi.org/10.1088/2053-1583/4/1/015043